

# Design of Induction Heatable Carbon-Based Foams for Catalysis

Jonathan Maier\*, Marc Greuel, Martin Hausrucking, Maximilian Oppmann, Clara Waterman and Benedikt Schug

DOI: 10.1002/cite.202300209

 This is an open access article under the terms of the [Creative Commons Attribution](https://creativecommons.org/licenses/by/4.0/) License, which permits use, distribution and reproduction in any medium, provided the original work is properly cited.

Carbon foams with and without functional particles were prepared via a simple direct foaming process. The carbon foams were composed of pyrolytic carbon and graphite. In the foams with additional functional particles, the latter were integrated directly in the direct foaming process. These functional particles were the catalytic material Saponite and the induction heat-able material MagSilica<sup>®</sup>. The foams were characterized including the induction heatability. The foams were also successfully tested in an induction heated lab-scale reactor for a case study reaction, ethanol to 1,3-butadiene.

**Keywords:** Catalysis, Carbon foam, Functional particles, Green chemistry, Induction heating

*Received:* October 23, 2023; *revised:* February 02, 2024; *accepted:* March 13, 2024

## 1 Introduction

Sustainable and green chemistry is becoming increasingly important. Therefore, the Fraunhofer project ShaPiD was initiated to enable green chemistry through practical technological innovations in process intensification and digitalization. Part of this project is the green production of olefinic monomer building blocks such as 1,3-butadiene (BD) from renewable raw materials.

Currently the main part of BD is produced with 95 % as a by-product during the thermal decomposition of naphtha to ethene [1]. As an alternative production process, BD synthesis from ethanol using catalysts is currently the subject of research [2–4]. Structured mesoporous support materials for catalysts are also being investigated. First results show that regularly ordered structures lead to an improvement of the catalysis process [5]. For this reason, catalysts using carbon foams as catalyst supports were used for this study.

Carbon foams have already been established for years as catalyst supports [6]. Usually, they are produced by chemical or physical direct foaming of different precursors, i.e., the introduction of gases, followed by carbonization or graphitization [7–9]. Another possibility is the pyrolysis of existing polymer foams [7]. Precursors used include pitch, coal, organic polymer resins and, more recently, sucrose, tannin and other natural carbon sources [7–9].

Induction heating is a new type of heating for catalytic applications. It is particularly useful for dynamic processes, because precisely defined temperatures can be reached fast and without contact. This enables new possibilities for reactor design [10–13]. The feasibility of combining catalysis and induction heating will be demonstrated in the project. For this purpose, so-called MagSilica<sup>®</sup> particles can be used

to specifically control the heatability in the catalytic process. The particles function as a very efficient susceptor to generate energy in an alternating field.

In brief, this study focused on the development of an inductively heatable and catalytically active carbon-based foam for BD synthesis. The production of such a foam should be performed via the relatively simple mechanical direct foaming process and two different drying methods, thermal drying and freeze drying. The possibility of directly incorporating the catalytic particles and the inductively heatable particles into the foam in this process was tested, and the foams produced were evaluated in the ethanol to BD (ETB) process.

## 2 Experimental

### 2.1 Preparation of Carbon Foams

The carbon foams were prepared using a mechanical direct foaming process following the patent DE102018200969B3/EP3514122A1 [13]. First, a solution of 1.25 wt % PureThix 1442 (BYK-Chemie GmbH, Germany) and deionized water

<sup>1</sup>Jonathan Maier  <https://orcid.org/0000-0003-2672-9775> ([jonathan.maier@isc.fraunhofer.de](mailto:jonathan.maier@isc.fraunhofer.de)), <sup>2</sup>Marc Greuel,

<sup>1</sup>Martin Hausrucking, <sup>1</sup>Maximilian Oppmann,

<sup>2</sup>Dr. Clara Waterman, <sup>1</sup>Dr. Benedikt Schug

<sup>1</sup>Fraunhofer ISC Zentrum HTL, Neunerplatz 2, 97082 Würzburg, Germany.

<sup>2</sup>Fraunhofer-Institut für Umwelt- Sicherheits- und Energietechnik UMSICHT, 46047 Oberhausen, Germany.

**Table 1.** Composition of foam masses for the production of carbon foams.

| Sample | Graphite [g] | Sugar [g] | Pure Thix solution [g] | Kelco Crete DG-F [g] | BWW40 [g] | PEG1000 [g] |
|--------|--------------|-----------|------------------------|----------------------|-----------|-------------|
| CFT    | 18           | 18        | 32                     | 0.32                 | 4         | -           |
| CFF1   | 18           | 18        | 32                     | 0.32                 | 4         | -           |
| CFF2   | 18           | 18        | 32                     | 0.32                 | 4         | 0.3         |
| CFF3   | 9            | 18        | 32                     | 0.32                 | 4         | 0.3         |
| CFF4   | 9            | 13        | 32                     | 0.32                 | 4         | 0.3         |

was prepared. A foam was produced from this solution by stirring at 1900 rpm with a dissolver disc (Dissolver Dispermat<sup>®</sup>, VMA-GETZMANN GmbH, Germany). A rheology additive (Kelco-Crete<sup>®</sup> DG-F U.S., Inc., CPKelco, USA), powdered sugar (Südzucker AG, Germany), cellulose fibers (Arbocel<sup>®</sup> BWW40, Kremer Pigmente GmbH & Co. KG, Germany), and in some cases a polyethylene glycol (PEG1000, Polyethylene glycol 10000 ROTIPURAN<sup>®</sup> Ph. Eur., Carl Roth GmbH + Co. KG) were added in this mechanical foaming process. Due to the addition of the individual additives, the viscosity of the foam mass increased. Afterwards, graphite powder (TIMREX E-SLS 30 GRAPHITE, Imerys S.A., France) and additional sugar were added. The compositions of the foam masses for the various carbon foams produced can be found in Tab. 1.

The prepared high-viscosity foam masses were filled into silicone molds (Ø 22 mm × 30 mm). Two different approaches were used to dry these foam masses. On the one hand, the foams were thermally dried (CFT) and, on the other hand, they were freeze-dried (CFF). In the case of thermal drying, the compounds were dried directly in the mold in a drying oven (LUT 5050 E, Heraeus Holding GmbH, Germany) at 70 °C. For freeze drying, the compounds were removed from the mold and frozen at -18 °C in a freezer. After 24 h in the freezer, the compounds were then freeze dried in a freeze dryer (Alpha 2-4, Martin Christ Gefriertrocknungsanlagen GmbH, Germany) at -60 °C for at least 48 h. After drying, all carbon foams were pyrolyzed in a high temperature graphite furnace (CAF 200/200\_2200G, MUT ADVANCED HEATING GmbH, Germany) at 1500 °C. The heating rate was 5 K min<sup>-1</sup> and the dwell time 6 h. The end faces were removed using a precision cutting machine (Accutom-10, Struers S.A.S., France) for the compressive strength measurements and the catalytic testing.

## 2.2 Preparation of Carbon Foams with Functional Particles

Functional particles were integrated into the foams. The functional particles were magnetic particles MagSilica<sup>®</sup> from Fraunhofer and a catalyst material (Saponite) for the syntheses in the reactor. MagSilica<sup>®</sup> is made of tailor-made

iron oxide nanoparticles with a silica shell. For the synthesis of the catalyst Saponite, sodium silicate (Na<sub>2</sub>SiO<sub>3</sub>) was dissolved in water (solution 1) and aluminum nitrate nona-hydrate (Al(NO<sub>3</sub>)<sub>3</sub>·9H<sub>2</sub>O) in 2 M NaOH (solution 2). The Si to Al ratio was always kept at 5.67 to 1.00. In a 20 L double wall reactor, solution 1 was provided and solution 2 was added under stirring. After a gelation, the gel was aged for 1 h at room temperature. Then, water was added and the suspension was heated to 90 °C before adding a solution consisting of magnesium nitrate hexa-hydrate (Mg(NO<sub>3</sub>)<sub>2</sub>·6H<sub>2</sub>O), urea (CH<sub>4</sub>N<sub>2</sub>O) and water. The heated reaction mixture was stirred for 20 h. Finally, the solid was filtered off, dried over night at 130 °C, milled in a ball mill and calcined at 400 °C for 3 h. A sieve fraction smaller 100 µm was prepared for further use.

To obtain carbon foams with functional particles inside of the foams they were introduced directly into the mechanical direct foaming process together with the graphite. The proportions of the functional particles in the foams are shown in Tab. 2. All foams with functional particles were produced according to the recipe of foam CFF4. The percentages refer to the theoretical carbon content in the finished pyrolyzed foam. For the addition of the functional particles, the graphite content and the sugar content were reduced in equal amounts in the foam masses. Drying was also performed by freeze-drying as for CFF4. Due to the stability of the functional particles, pyrolysis of the foams was carried out at 400 °C.

For the preparation of induction heatable pellets 50 % MagSilica<sup>®</sup>, 30 % ceramic material and 20 % Saponite were mixed. An extrusion mass was prepared and extruded into

**Table 2.** Proportions of the respective functional particles in the carbon foams.

| Sample      | Saponite [wt %] | MagSilica <sup>®</sup> [wt %] |
|-------------|-----------------|-------------------------------|
| CFF-15S     | 15              | -                             |
| CFF-15M     | -               | 15                            |
| CFF-50M     | -               | 50                            |
| CFF-15S-15M | 15              | 15                            |

pellets using a single screw extrusion system (KEP-20-20-S-K, Ematik GmbH, Germany). The resulting pellets were dried for 7 h at 35, 55, 85 and 105 °C, respectively. The pellets were then heated to 350 °C (heating rate 5 °C min<sup>-1</sup>) in nitrogen atmosphere (100 mL min<sup>-1</sup>).

## 2.3 Characterization of Foams

The pore size distribution and the specific pore volume were measured by 3P INSTRUMENTS GmbH & Co. KG using mercury porosimetry (Quantachrome Poremaster 60-GT) according to the norm ISO 15901-1. The samples were pre-treated at 105 °C for 2 h in a drying oven. The compressive strength of the carbon foams was determined using a material testing machine (Zwick Z100, Zwick Roell AG, Germany) following the norm DIN51910. The force was measured using a 20 kN load cell. The measurements were done with a preload of 0.2 N and a test speed of 1 mm min<sup>-1</sup>. The microstructure of the foams was examined using a scanning electron microscope (SEM, Supra25, Carl Zeiss AG, Germany). The backscattered electron detector (BSD), the secondary electron detector (SE) and the in-lens detector were used for the analysis.

### 2.3.1 Induction Heating

A high frequency induction system (SINUS 102, HIM-MELWERK Hoch- und Mittelfrequenzanlagen GmbH, Germany) with an internally cooled inductor was used for heating of the various foam materials. The inductor consisted of a round coil with three turns, an inner diameter of 3 mm and a coil height of 75 mm. The coil winding thickness was 5 mm in diameter. A glass tube could be inserted inside the inductor to serve as the vessel of the actual plug-flow reactor (see Fig. 1). In the case of the experiments without the synthesis reactor, the experiments were also carried out without a glass tube in air to measure the temperature of the foams directly on the foam surface. The temperature was measured using an infrared thermometer (optrics CTlaser LT, Optrics GmbH, Germany). Two different heating capacities, 50 % and 90 %, were used for these tests. The inductive heatability of pellets was also determined in addition to the foams for comparison.

## 2.4 Catalytic Testing

The conventional conversion of ethanol to butadiene was investigated in a continuous flow, fixed bed stainless steel double tube reactor with a 10 mm inner diameter of the catalyst containing tube and a total outer diameter of 28 mm. A stainless-steel frit was placed as a support area for the catalyst 330 mm from the top of the inner tube. The catalyst was fixed between two glass wool plugs on top of the frit. For the testing of the catalytic activity powdered carbon foams (2.23 g, 100–250 μm) were used. For testing the



**Figure 1.** Experimental setup of reactor for catalytic testing in combination with induction heating. A carbon foam is placed inside of the inductor.

catalyst in the inductive setup, a quartz glass tube of 350 mm length and an inner diameter of 19 mm was used. The glass reactor was clamped between two heatable aluminum blocks through which the gas flow was directed through the reactor. The carbon foams (2.1–2.4 g) were placed on top of glass wool inside the inductor. Temperature measurement and control could not be applied during induction testing.

Prior to the activity test, two by-pass measurements were performed to determine the initial ethanol concentration ( $c_{EtOH, i}$ ). Reaction parameters for the conventional catalytic tests were  $T = 200\text{--}450$  °C,  $WHSV = 1.0$ , and  $1.5$  h<sup>-1</sup>,  $TOS = 0.75$  h, as well as  $V = 100$  mL min<sup>-1</sup> with 5 mol % ethanol in nitrogen for the pellets and the carbon foams, respectively. The capacity in the inductive catalytic tests was 90 %.

The composition of the product mixture was determined using an inline gas chromatograph (GC 2014, Shimadzu Corporation, Japan) equipped with a flame ionization detector (FID) and a thermal conductivity detector (TCD). For the separation of the samples, an SH Rxi 624Sil MS column (30 m × 0.25 mm × 1.4 μm) and a combination of a PorapakQ 1 and a Molsieve 5a column (4 m × 2 mm) were used, respectively. The conversion of ethanol  $X_C$  was determined based on the carbon number in the initial ethanol flow ( $2\dot{n}_{EtOH, 0}$ ) and the carbon number in the remaining

ethanol ( $2\dot{n}_{EtOH,i}$ ) at the respective temperature or voltage  $i$  (Eq. (1)). For temperatures/voltages without unknown products the product selectivity for a component  $a$   $S_{P,a}$  (Eq. (2)) was calculated based on the carbon number of all products  $\sum_1^a n_{C,a} \cdot \dot{n}_{a,i}$  with  $n_{C,a}$  equal to the number of carbons in the component  $a$  and  $\dot{n}_{a,i}$  the molar flow of component  $a$  at the respective temperature/voltage  $i$ .

$$X_C = \frac{2(\dot{n}_{EtOH,0} - \dot{n}_{EtOH,i})}{2\dot{n}_{EtOH,0}} \cdot 100 \quad (1)$$

$$S_{P,a} = \frac{n_{C,a} \dot{n}_{a,i}}{\sum_1^a n_{C,a} \dot{n}_{a,i}} \cdot 100 \quad (2)$$

For higher temperatures with unidentified products in the product stream, the carbon-based selectivity for component  $a$   $S_{C,a}$  was calculated using Eq. (3).

$$S_{C,a} = \frac{n_{C,a} \cdot \dot{n}_{a,i}}{2(\dot{n}_{EtOH,0} + 2\dot{n}_{EtOH,i})} \cdot 100 \quad (3)$$

The unknown products can be observed as the difference between the expected 100 % selectivity and the calculated total selectivity of the known products. The standard error on the conversion was determined using Gaussian error propagation starting from the error in the ethanol area measured by GC-FID.

## 3 Results and Discussion

### 3.1 Preparation of Carbon Foams

Carbon foams were prepared using different formulations in combination with mechanical direct foaming and different drying methods. Fig. 2 shows the image of a carbon foam produced by the direct foaming process and in combination with freeze drying and a subsequent pyrolysis. After shrinkage by pyrolysis, the foams had a diameter of approximately 18 mm, which was intended for application in the catalytic reactor. Analyses were performed on these foams.

In Fig. 3, the pore size distribution of the carbon foams is shown. The goal was to adapt foams with pore sizes in the area around 100  $\mu\text{m}$  and more open porosity so that the foams would be suitable support materials for the catalysts. It can be seen that the freeze-dried foams CFF1 had a narrower pore size distributions with larger modal values compared to the thermally dried foams CFT. The thermally dried foams also showed very large pores in the millimeter range. However, cracks and large bubbles appeared in the freeze-dried foams due to the freezing process. The addition of polyethylene glycol to the CFF2 foam prevented this without having a significant effect on the pore size distribution. Therefore, freeze-drying was more suitable for producing foams with defined pore size distributions after the addition of polyethylene glycol. Thus, all further foams were dried by freeze-drying and for further adjustments, the composition



Figure 2. Image of a carbon foam.

of the foam masses was varied. The reduction of the graphite content in foam CFF3 resulted in larger pores compared to CFF2.

A further adaptation of the foam mass composition by reducing the sugar content for foam CFF4 did not show any significant change in the pore size distribution. However, compared to the foams CFT, CFF1, CFF2 and CFF3, a higher specific pore volume was achieved, see Tab. 3. In other words, foam CFF4 had a higher open porosity. Tab. 3 also shows the compressive strengths of the different foams. The thermally dried foam had the highest strength at 5.9 MPa. The freeze-dried foams showed a reduced strength

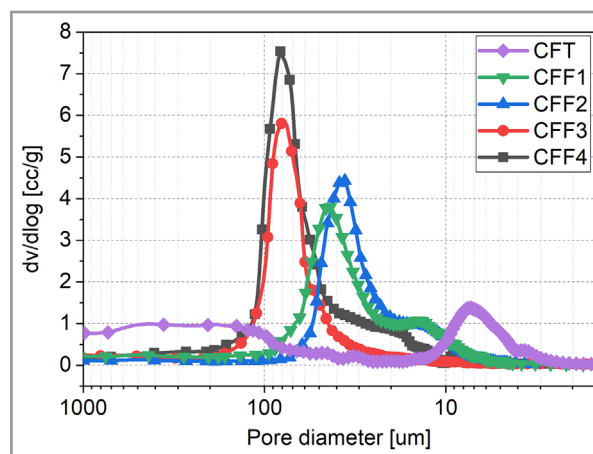


Figure 3. Pore size distribution of carbon foams with different which were produced with different formulations and drying processes.

**Table 3.** Specific pore volume and compressive strength of carbon foams.

| Sample | Specific pore volume [cm <sup>3</sup> /g] | Compressive strength [MPa] |
|--------|---|----------------------------|
| CFT    | 1.61                                      | 5.9 ± 1.2                  |
| CFF1   | 1.89                                      | 2.8 ± 0.2                  |
| CFF2   | 1.75                                      | 2.2 ± 0.1                  |
| CFF3   | 1.82                                      | 2.2 ± 0.6                  |
| CFF4   | 2.75                                      | 1.5 ± 0.2                  |

of 2.8 MPa and the addition of PEG also resulted in a slight reduction to 2.2 MPa. This is due to the finer and more homogeneous pore network compared to the foam CFT. The foam CFT had large pores but relatively compact cell walls and struts. However, a large proportion of the CFT foams had large pores in the range of several millimeters, which could not be used for compressive strength measurements. The strength was also further reduced to 1.5 MPa for the foam with increased open porosity. However, due to its more suitable pore structure, the CFF4 foam was chosen as a starting point for the production of foams with functional particles.

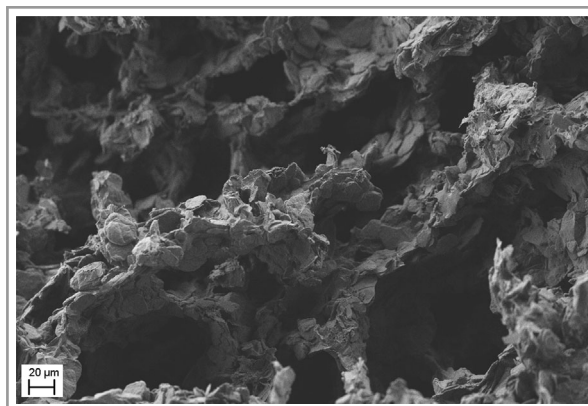
The compressive strength of carbon foams with functional particles was also studied and the results are shown in Tab. 4. Compared to the foams without functional particles, all foams showed a reduction in compressive strength. However, the foams had sufficient strength for the application.

Fig. 4 shows the SEM image of the carbon foam CFF4. It can be seen that the cell walls and struts of the foam are largely composed of graphite flakes held together by the pyrolytically produced carbon.

Fig. 5 shows the foams CFF-15S and CFF-15S-15M with functional particles. The pore size as well as the foam structure of CFF-15S show no significant difference compared to CFF4. The backscattered electron detector image shows that the particles were incorporated into the foam network. Furthermore, some of the Saponite particles were accessible and not encapsulated by carbon or graphite. Foam CFF-15S-15M also had the same pore structure and comparable pore sizes. In Fig. 5c, however, a section is shown that represents more the wall and strut structure to show a more accurate picture of the particle distribution in the foam. In addition

**Table 4.** Compressive strength of carbon foams.

| Sample      | Compressive strength [MPa] |
|-------------|----------------------------|
| CFF-15S     | 0.59 ± 0.02                |
| CFF-15M     | 0.50 ± 0.02                |
| CFF-50M     | 0.47 ± 0.04                |
| CFF-15S-15M | 0.44 ± 0.06                |



**Figure 4.** SEM image (SE detector) of carbon foam CFF4.

to pyrolytic carbon, graphite, and Saponite, this foam also contained MagSilica<sup>®</sup> particles. These can be seen in the BSD image in Fig. 5d. The nanometer-sized MagSilica<sup>®</sup> particles have a high brightness in the image compared to carbon and Saponite and were located on the surface and between the graphite and Saponite particles.

### 3.2 Induction Heating

The induction heating capability of various foams was measured and compared with composite pellets (magnetite, Saponite, ceramic), which have so far been used as the standard material. Fig. 6 shows thermal camera images of the induction heating process after 0 s, 60 s and 300 s.

The heating curves with two different heating powers are shown in Fig. 7. At a heating power of 50 %, the carbon foam CFF4 without additional functional particles showed an immediate increase in temperature above 800 °C. The rapid heating of the pure graphite foam is based on the heating behavior due to the Joule effect produced by eddy currents [14]. In comparison, all foams with additional functional particles and the pellets heated up more slowly or showed almost no temperature increase. The latter include the foams CFF15S CFF15M and CFF15S-15M and the pellets. In contrast, the foam CFF50M with a higher content of MagSilica<sup>®</sup> showed a slow heating up to approx. 180 °C and then a rapid heating step up to 480 °C. The foam then remained constant at this temperature. This temperature step was also similar for the pellets, but was flatter in comparison. In the samples with magnetic particles, heating is achieved by hysteresis losses. The magnetism is adjusted so that the hysteresis area, which is proportional to the available energy, is as large as possible to generate good heating power. However, if the coercive field strength in the alternating field exceeds the field strength of the induction field, excitation is no longer possible. The coercivity is not a static quantity but depends on the frequency of the induction field and the temperature. Therefore, the coercive field strength

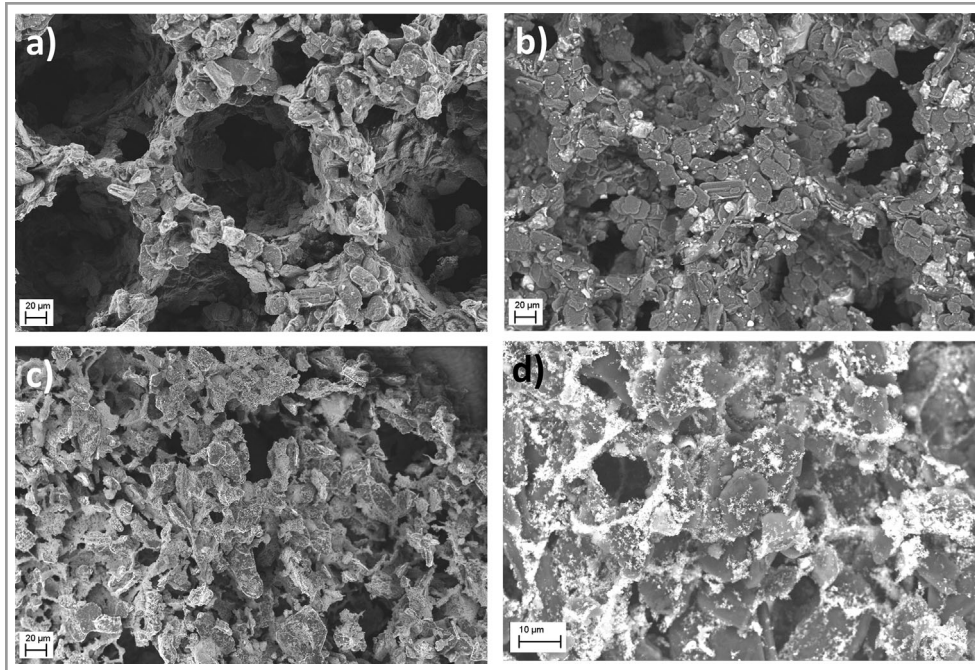


**Figure 5.** SEM images of carbon foams. a) CFF-15S (SE detector), b) CFF-15S (BSD detector), c) and d) CFF-15S-15M (in-lens detector).



**Figure 6.** Thermal camera images of induction heating process of the carbon foam CFF-50M.

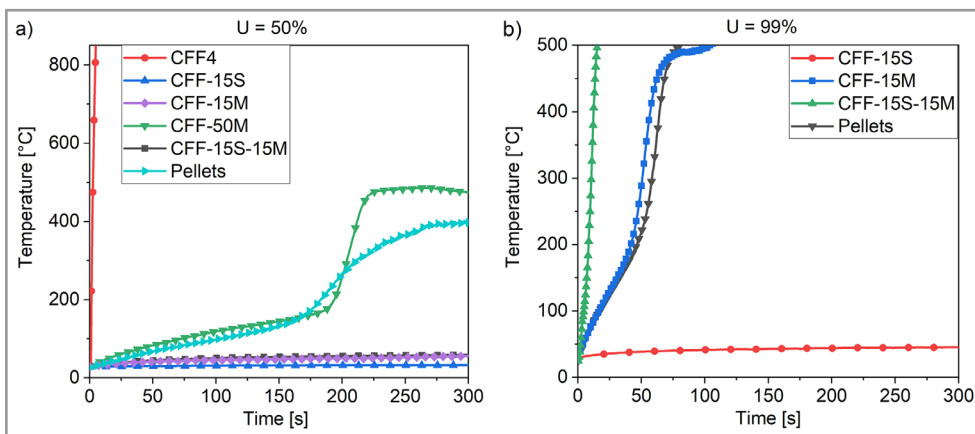


**Figure 7.** Induction heating with 50 % (a) and 99 % (b) heating capacity.

tends to increase at high frequencies and to decrease with increasing temperatures [15, 16]. In the measurements, this behavior is evident by an increase in the slope of the curves at about 200 s. Due to a widening of the hysteresis at high frequencies, the heating of the optimized susceptors was initially lower. With increasing temperatures, however, the coercivity decreases again and the heating performance increases from approx. 150–180 °C onwards. Therefore, by optimizing the frequency and field strength, a good heating performance can be directly realized in a commercial application. This effect is also evident in the heating curves of the foam CFF-15M and the pellets with 99 % heating capacity. In this case, however, it is less pronounced due to the generally faster heating caused by the higher heating power. With the higher heating power, it is possible to heat foams that could not be heated with the lower heating power. The foam CFF-15S-15M with Saponite and MagSilica® even showed a rapid increase in temperature at the start of heating at this heating capacity comparable to the rapid heating of CFF4 at the lower heating capacity. This means that at the higher heating power, the foams could generally be heated more effectively. Only Foam CFF-15S without MagSilica® showed no heatability at all.

### 3.3 Catalytic Activity

The influence of indirect (conventional) and direct (inductive) heating on the catalytic performance of foams and pellets with integrated Saponite in the ETB reaction was investigated. The results of the catalytic activity of carbon foams with functional particles as well as conventional indirect and inductive direct heating are compared in the following section.

#### 3.3.1 Catalytic Performance with Indirect Heating of Carbon-Based Foam

Fig. 8 shows the results of the catalytic ETB process with Saponite powder diluted with  $\alpha$ -Al<sub>2</sub>O<sub>3</sub> (Fig. 8a) and the powdered CFF-15S-15M foam (Fig. 8b). The results show a conversion of 62 % at 300 °C and full conversion at 400 °C for the Saponite powder. In contrast, the powdered CFF-15S-15M shows a conversion level of 59 % only at 400 °C, while full conversion with 90 % is still not achieved at 450 °C. These results can be attributed either to the increase in the WHSV from 1 h<sup>-1</sup> to 1.5 h<sup>-1</sup> or to the inclusion of catalyst material in the foam material. The inclusion of catalyst material can lead to a decrease in the availability of catalytic sites as well as diffusion limitations. Moreover, the product composition for the two materials was different. For Saponite, the main products at the lower temperatures of 200–300 °C were diethyl ether (DEE) and ethene, and at the higher temperatures of 350–450 °C, ethene was the main product. A low 1,3-butadiene selectivity of 2 % was achieved for 350–450 °C. In comparison, the powdered CFF-15S-15M

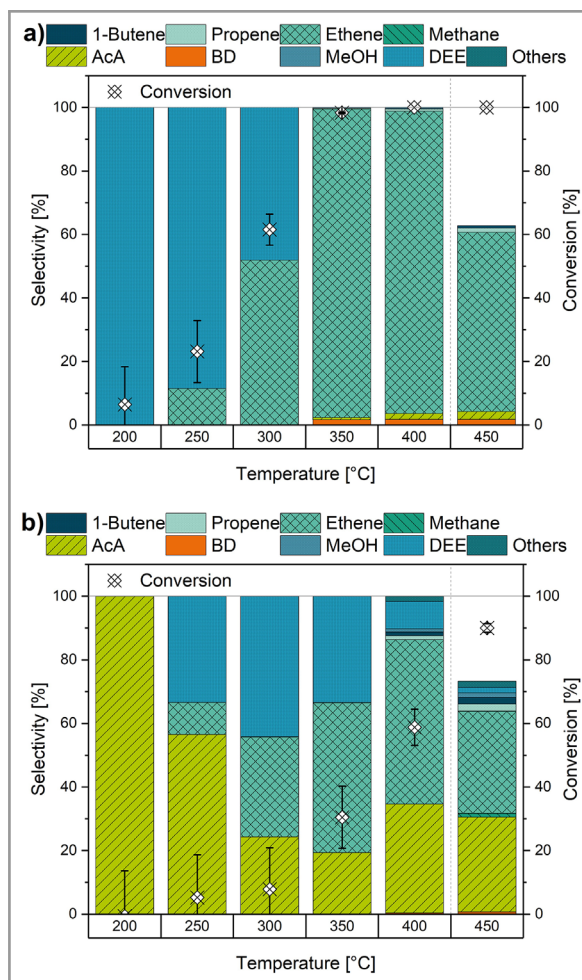


**Figure 8.** Product selectivity and conversion for the ETB reaction with a) 0.5 g Saponite powder diluted with 2.5 g  $\alpha$ -Al<sub>2</sub>O<sub>3</sub> (WHSV = 1 h<sup>-1</sup>), b) powdered CFF-15S-15M foam (2.2 g, 100–250  $\mu$ m fraction, WHSV = 1.5 h<sup>-1</sup>) in the conventional reactor, reaction parameters  $T = 200$ –450 °C,  $p = 1$  bar, TOS per  $T = 0.75$  h, the dashed vertical line marks the calculation change between  $S_{p,a}$  and  $S_{c,a}$ .

showed a high acetaldehyde (AcA) selectivity above 19 % for the whole temperature range with DEE and ethene as the main by-products above 250 °C. In addition, the BD selectivity was reduced, showing no BD at 350 °C and only 1 % BD for 400 and 450 °C.

These results suggest that the other foam components MagSilica® and carbon also had an influence on the catalytic activity. The catalytic results of MagSilica® powder in the conventional setup confirmed its catalytic activity in the conversion of ethanol as shown in Fig. 9. For MagSilica®, the main product was AcA, with a selectivity above 50 % for all known products.

Moreover, carbon additives do not show a catalytic activity for ethanol conversion as will be shown elsewhere. These results lead to the assumption, that MagSilica® mainly provides catalytic active sites for the oxidation of ethanol to

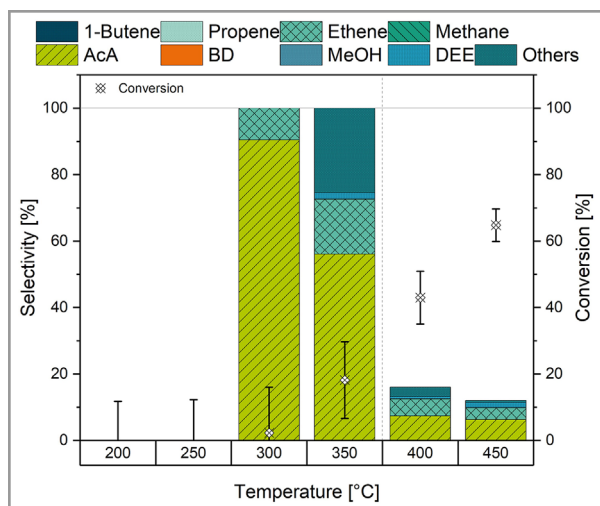


**Figure 9.** Product selectivity and conversion for the ETB reaction with 0.5 g MagSilica® diluted with 2.5 g  $\alpha$ -Al<sub>2</sub>O<sub>3</sub> in the conventional reactor, reaction parameters  $T = 200\text{--}450$  °C,  $WHSV = 1\text{ h}^{-1}$ ,  $p = 1$  bar, TOS per  $T = 0.75$  h, the dashed vertical line marks the calculation change between  $S_{p,a}$  and  $S_{c,a}$ .

AcA. For the use of inductive heating in heterogeneous catalysis, this concludes that the choice of additives as well as the catalyst is very important to avoid altering the materials catalytic activity and undesirable side reactions.

### 3.3.2 Influence of Heating Method on Carbon-Based Foam in the Catalytic Conversion of Ethanol to Butadiene

The influence of the heating method (conventional and inductive) was investigated. Therefore, three CFF-15S-15M foams were tested with an inductively heated reactor setup ( $WHSV = 1.5\text{ h}^{-1}$ ,  $U = 90\%$ ). The catalytic tests had a good reproducibility, and the results are shown in Fig. 10. A conversion of  $85\% \pm 2\%$  was observed with a product composition mainly consisting of AcA (16%), methane (6%) and ethene (30%). Despite a low BD selectivity below 1%, the desired product was still detected.

Comparing the catalytic results of the conventional heating with the inductive heating, the product composition at these conversion rates ( $\sim 85\text{--}90\%$ ) was similar, containing mainly methane, ethene and AcA. Thus, the heating method has no effect on the catalytic activity of the material.

## 4 Conclusions

A manufacturing route for carbon foams with additional functional particles was successfully developed. It was possible to produce foams by a simple mechanical direct foaming route. The open porosity was controlled by the composition of the foam masses. Functional particles were

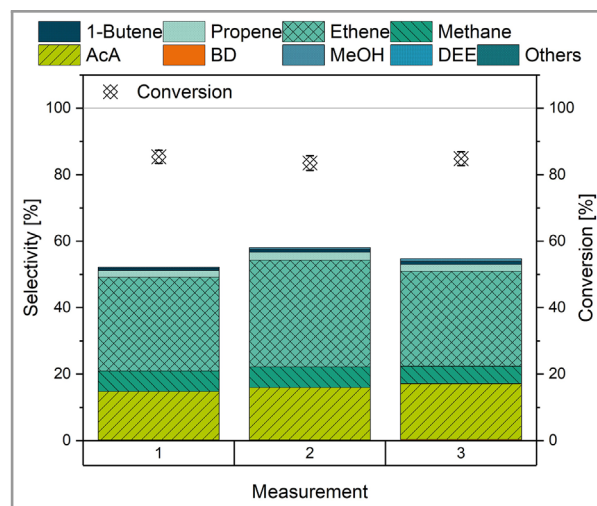


**Figure 10.** Product selectivity and conversion for the ETB reaction with CFF-15S-15M foams in the inductive reactor, reaction parameters  $WHSV = 1.5\text{ h}^{-1}$ ,  $U = 90\%$ ,  $l = 14\%$ ,  $f = 1070$  Hz,  $p = 1$  bar, TOS per  $T = 0.75$  h, product selectivity  $S_{c,a}$  was calculated based on ethanol conversion.

directly integrated into the foams during the direct foaming process and were homogeneously distributed throughout the foams after the final heat treatment.

The induction heating process showed that pure carbon foams can be heated to high temperatures within a very short time at low heating powers. However, the effect of thermally induced mechanical stresses on the service life of the foams is small, because of the low coefficient of thermal expansion of carbon or graphite [17, 18]. The atmosphere, on the other hand, is decisive for a future application and their service life. In oxygen-containing atmospheres, it must be taken into account that graphite and pyrolytic carbon begin to oxidize at temperatures above 400 °C [19, 20]. Foams with a high proportion of inductively heatable particles could also be heated. In this case, however, the heating was slower and therefore easier to control. All foams with a lower proportion of functional particles could not be heated at low capacities. At high heating powers, on the other hand, all foams with magnetic particles could be heated.

The foams were tested for their catalytic activity in the conversion of ethanol to BD in a conventional and inductive reactor setup. It was observed when using inductively heatable catalysts that equivalent product compositions could be obtained comparing conventional and inductive heating. For further investigations, it will be necessary to implement a temperature control and a substrate gas preheating in the inductive setup. Moreover, for the evaluation of the energy input, the reactor setups require the same insulation around the reactor to avoid energy losses and to obtain comparable results. Despite the low selectivity towards BD, it was shown that BD can be obtained with this catalyst. In further steps, the catalyst will also be adapted to achieve a higher yield

of butadiene (up to 70–73 %) comparable to the results reported in the current literature [21–24].

## Acknowledgment

The authors thank 3P INSTRUMENTS GmbH & Co. KG for the measurements of the pore size distribution.

Open access funding enabled and organized by Projekt DEAL.

## Abbreviations

|      |                                 |
|------|---------------------------------|
| BD   | Butadiene                       |
| BSD  | Backscattered electron detector |
| FID  | Flame ionization detector       |
| GC   | Gas chromatograph               |
| SE   | Secondary electron detector     |
| SEM  | Scanning electron microscope    |
| T    | Temperature                     |
| TCD  | Thermal conductivity detector   |
| TOS  | Time-on-stream                  |
| WHSV | Weight hourly space velocity    |

## References

- [1] W. C. White, *Chem.-Biol. Interact.* **2007**, *166* (1–3), 10–14. DOI: <https://doi.org/10.1016/j.cbi.2007.01.009>
- [2] G. Pomalaza et al., *Catal. Sci. Technol.* **2020**, *10* (15), 4860–4911. DOI: <https://doi.org/10.1039/D0CY00784F>
- [3] S. A. Akhade et al., *J. Catal.* **2020**, *386*, 30–38. DOI: <https://doi.org/10.1016/j.jcat.2020.03.030>
- [4] L. Qi et al., *J. Am. Chem. Soc.* **2020**, *142* (34), 14674–14687. DOI: <https://doi.org/10.1021/jacs.0c06906>
- [5] C.-I. Ahn et al., *Fuel Process. Technol.* **2020**, *200*, 106317. DOI: <https://doi.org/10.1016/j.fuproc.2019.106317>
- [6] F. Glenk et al., *Chem. Eng. Technol.* **2010**, *33* (4), 698–703. DOI: <https://doi.org/10.1002/ceat.201000005>
- [7] N. C. Gallego, J. W. Klett, *Carbon* **2003**, *41* (7), 1461–1466. DOI: [https://doi.org/10.1016/S0008-6223\(03\)00091-5](https://doi.org/10.1016/S0008-6223(03)00091-5)
- [8] C. Chen, et al., *Carbon* **2006**, *44* (8), 1535–1543. DOI: <https://doi.org/10.1016/j.carbon.2005.12.021>
- [9] A. Chithra et al., *Ind. Crops Prod.* **2020**, *145*, 112076. DOI: <https://doi.org/10.1016/j.indcrop.2019.112076>
- [10] S. Ceylan et al., *Chem. – Eur. J.* **2011**, *17* (6), 1884–1893. DOI: <https://doi.org/10.1002/chem.201002291>
- [11] B. Seo, S. H. Joo, *Nat. Energy* **2018**, *3* (6), 451–452. DOI: <https://doi.org/10.1038/s41560-018-0157-5>
- [12] C. Niether et al., *Nat. Energy* **2018**, *3* (6), 476–483. DOI: <https://doi.org/10.1038/s41560-018-0132-1>
- [13] E. H. Hoffmann, J. Vogt, T. Martini, *EU Patent 3514122 (A1)*, **2019**.
- [14] B. Patidar et al., *IET Electric Power Applications* **2017**, *11* (3), 342–351. DOI: <https://doi.org/10.1049/iet-epa.2016.0393>
- [15] G. Cotin et al., *Nanomater. Magn. Opt. Hyperthermia Appl.* **2019**, 41–60. DOI: <https://doi.org/10.1016/B978-0-12-813928-8.00002-8>
- [16] X. Yu et al., *Sci. Rep.* **2022**, *12* (1), 16055. DOI: <https://doi.org/10.1038/s41598-022-20558-0>
- [17] W. Zhang et al., *ZAMM* **2013**, *93* (5), 338–345. DOI: <https://doi.org/10.1002/zamm.201100132>
- [18] L. Zhao et al., *New Carbon Mater.* **2022**, *37* (3), 544–555. DOI: [https://doi.org/10.1016/S1872-5805\(22\)60603-6](https://doi.org/10.1016/S1872-5805(22)60603-6)
- [19] L. Wiaowei, J.-C. Robin, Y. Suyuan, *Nucl. Eng. Des.* **2004**, *227* (3), 273–280. DOI: <https://doi.org/10.1016/j.nucengdes.2003.11.004>
- [20] R. R. Naslian, *Composites, Part A* **1998**, *29* (9–10), 1145–1155. DOI: [https://doi.org/10.1016/S1359-835X\(97\)00128-0](https://doi.org/10.1016/S1359-835X(97)00128-0)
- [21] T. de Baerdemaeker et al., *ACS Catal.* **2015**, *5* (6), 3393–3397. DOI: <https://doi.org/10.1021/acscatal.5b00376>
- [22] A. D. Winkelmann et al., *Catal. Sci. Technol.* **2023**, *13* (4), 975–983. DOI: <https://doi.org/10.1039/d2cy01722a>
- [23] V. L. Dagle et al., *Appl. Catal., B* **2018**, *236*, 576–587. DOI: <https://doi.org/10.1016/j.apcatb.2018.05.055>
- [24] H. Dai et al., *Catalysts* **2022**, *12* (10), 1147. DOI: <https://doi.org/10.3390/catal12101147>